Estimate of the rigidity of eclogite in the lower mantle from waveform modeling of broadband S-to-P wave conversions

Samuel M. Haugland[1]*, **Jeroen Ritsema**[1]

Satoshi Kaneshima[2]

Michael S. Thorne[3]

[1]Department of Earth and Environmental Sciences, University of Michigan, Ann Arbor, Michigan, USA.
[2]Department of Earth and Planetary Sciences, Kyushu University, Fukuoka, Japan
[3]Department Geology and Geophysics, University of Utah, Salt Lake City, Utah, USA.

Key Points:

- Broadband seismometers in western North America recorded a S-to-P conversion at 1750 km depth beneath northwestern South America.
- Finite-difference waveform modeling suggests $S_{1750}P$ was formed by a 10-km thick heterogeneity with a shear-velocity reduction between -1.6% and -12.4%.
- Our results are consistent with ab initio calculations of shear softening due to the post-stishovite phase transition in subducted mid-ocean ridge basalt.

*Current address, 2534 C.C. Little Building, 1100 N. University Ave., Ann Arbor, Michigan

Corresponding author: Samuel Haugland, samhaug@umich.edu

Abstract

Broadband USArray recordings of the July 21, 2007 western Brazil earthquake (M_W = 6.0; depth = 633 km) include high-amplitude signals about 40 s, 75 s, and 100 s after the P wave arrival. They are consistent with S-wave to P-wave conversions in the mantle beneath northwestern South America. The signal at 100 s, denoted as $S_{1750}P$, has the highest amplitude and is formed at 1750 km depth based on slant-stacking and semblance analysis. Waveform modeling using axisymmetric, finite-difference synthetics indicates that $S_{1750}P$ is generated by a 10-km thick heterogeneity, presumably a fragment of subducted mid-ocean ridge basalt in the lower mantle. The negative polarity of $S_{1750}P$ is a robust observation and constrains the shear-velocity anomaly δV_S of the heterogeneity to be negative. The amplitude of $S_{1750}P$ indicates that δV_S is in the range from -1.6% to -12.4%. The large uncertainty in δV_S is due the large variability in the recorded $S_{1750}P$ amplitude and simplifications in the modeling of $S_{1750}P$ waveforms. The lower end of our estimate for δV_S is consistent with ab initio calculations by *Tsuchiya* [2011], who estimated that δV_S of eclogite at lower-mantle pressure is between 0 and -2% due to shear softening from the post-stishovite phase transition.

1 Introduction

While seismic tomography has mapped the penetration of subducting lithosphere into the lower mantle on scales > 100 km [e.g., *Grand et al.*, 1997; *Fukao et al.*, 2001], array recordings of reflected or converted phases indicate fine-scale (10–100 km) structure is present in the deep mantle [e.g., *Shearer*, 2007; *Kaneshima*, 2016]. S-to-P conversions at depth x, denoted as SxP, are excellent probes for detecting layering or localized heterogeneity in the lower mantle beneath deep-focus earthquakes. These shear-wave conversions have been used to map small-scale seismic structure beneath the Marianas [e.g., *Kaneshima & Helffrich*, 1998], Tonga [e.g., *Kaneshima*, 2013; *Li & Yuen*, 2014; *Yang & He*, 2015], Indonesia [e.g., *Kawakatsu & Niu*, 1994; *Niu & Kawakatsu*, 1997; *Vinnik et al.*, 1998; *Vanacore et al.*, 2006], South America [e.g., *Castle & van der Hilst*, 2003; *Kaneshima & Helffrich*, 2010], and northeast China [*Niu*, 2014]. *Kaneshima & Helffrich* [1999] interpreted these small-scale, deep mantle heterogeneities as fragments of subducted oceanic crust.

We inspected Transportable Array (TA) and Canadian National Seismic Network (CNSN) waveforms from 41 deep-focus (> 300 km) earthquakes in South America since

1990. We detected high-amplitude S*x*P conversions only in recordings of the July 21, 2007 $M_W = 6.0$ (latitude = 8.1°S; longitude = 71.3°W; depth = 633 km) western Brazil earthquake (the Brazil earthquake from hereon). The Brazil earthquake had a dip-slip source mechanism with optimal downward radiation of SV-polarized shear-waves. The absence of clear S-P conversions in waveform data from other events is likely due to the unique focal mechanism of the Brazil earthquake.

Previous studies have modeled the amplitude and polarity of S-P conversions [e.g., *Vinnik et al.*, 1998; *Kaneshima & Helffrich*, 1999; *Niu*, 2014]. In this paper we analyze broadband regional network waveforms by 2D finite difference modeling at periods longer than 2 seconds. The broadband recording of $S_{1750}P$ at stations from the TA and CNSN elucidates the signal polarity and amplitude. By forward waveform modeling, we put constraints on the thickness and the shear velocity of the anomalous structure in the deep mantle responsible for generating $S_{1750}P$.

2 S*x*P conversions in the lower mantle beneath South America

2.1 Wave geometry

S*x*P is formed when the downward propagating S wave converts to a P wave at a discontinuity or heterogeneity in seismic velocity at depth *x* below the earthquake source. Beneath the Brazil earthquake, S*x*P conversions form in a high-velocity structure that we interpret as the Nazca lithosphere subducted beneath western South America (Figure 1). We can distinguish S*x*P from crustal reverberations and reflections off boundaries above the earthquake (i.e., $p_{410}P$, $s_{410}P$) or beneath the receivers (e.g., $P_{410}s$, $P_{660}s$) when its slowness can be determined using recordings from a wide-aperture network.

2.2 Waveforms from North America

More than 250 TA and CNSN stations in western North America recorded the Brazil earthquake between 56° and 73°. The record section of vertical-component traces in Figure 2a shows the ground velocity after alignment on the P-wave (at time 0). The seismic phases PcP and pP are reflections off the outer core and Earth's surface, respectively. Three S_xP signals at about 45 s, 75 s, and 100 s after the P arrival, are visible throughout the section.

The signals at 45 s, which may interfere with $p_{410}P$, and at 75 s are $S_{950}P$ and $S_{1250}P$, respectively. These conversions were formed about 3° off the great-circle path and have complex waveforms (see Figure S1).

We interpret the impulsive arrival at 100 s as $S_{1750}P$. Its arrival time decreases with increasing epicentral distance with respect to P, as expected for a S*x*P conversion.

The vespagram in Figure 2b indicates that the slowness of $S_{1750}P$ is about 0.2 s/° higher than predicted for a standard 1-D seismic model. This suggests that the $S_{1750}P$ conversion point is located further from the earthquake hypocenter than expected for a 1-D wave speed model. Semblance is a measure of coherent energy in a stack of data arriving from a common conversion point. By semblance analysis, following *Kaneshima & Helffrich* [2003], we locate the conversion point of $S_{1750}P$ between 1700 and 1750 km depth within the sector of source azimuths of the TA and CNSN stations but about 400 km to the NW of the 1-D predicted conversion location (Figure 2c). This is consistent with the $S_{1750}P$ slowness and traveltime observed in Figure 2b.

3 Waveform modeling

The $S_{1750}P$ signal is recorded above noise level in 30 vertical displacement seismograms from the TA and CNSN. Figure 3 shows these waveforms and their sum after they have been aligned and scaled such that the SV wave, which converts into $S_{1750}P$, has an amplitude equal to 1. The $S_{1750}P$ signal in each of these 30 records is comprised of a negative and a positive pulse separated by about 2 s, with varying amplitudes. The mean value of the peak-to-peak amplitude is 4.4% of the SV amplitude on the vertical component and the two-standard deviation of the amplitude is 3.4%.

Computed waveforms indicate that the waveform shape of $S_{1750}P$ is due to the interference of two S-to-P conversions at the upper and lower boundaries of a narrow velocity structure. These two conversions have opposite polarities. We model the heterogeneity that produces $S_{1750}P$ as a block centered on the ray-theoretical $S_{1750}P$ conversion point beneath the earthquake (Figure 4a). The block has a thickness h and makes an angle α with the equatorial plane.

We choose long blocks to avoid wave diffraction around them. We expect diffraction to reduce the amplitude of $S_{1750}P$ but it must be studied in 3-D. The S-wave velocity contrast with respect to the ambient mantle is δV_S. Our synthetics indicate that anomalies in the P-wave velocity and density do not affect the $S_{1750}P$ waveform significantly See Figure S2.

We model the stack of the 30 high-amplitude $S_{1750}P$ waveforms using synthetics computed with the PSVaxi method [e.g., *Thorne et al.*, 2013], a finite-difference method similar to the SHaxi method developed by *Jahnke et al.* [2008]. PSVaxi allows us to compute the full seismic wavefield of P-SV motions with the correct 3-D geometric spreading for a model of seismic structure in the plane of the great-circle arc. The 2-D grid of heterogeneity is expanded to 3-D spherical geometry by rotating it around the radial axis passing through the seismic source. Our PSVaxi synthetics include signals up to frequencies of 0.5 Hz (i.e., a shortest dominant period of 2 s) but, due to the assumed axisymmetry, signals from off-azimuth wave propagation or SH-to-P conversions cannot be modeled.

We compute synthetics for the PREM seismic model and for a 3-D model in which the block heterogeneity at 1750 km depth is embedded within PREM. In the PREM model, we replace the 220-km, 400-km and 670-km discontinuities by smooth gradients to suppress reflections and conversions produced in the upper mantle. We subtract the PREM and 3-D waveforms to isolate the $S_{1750}P$ signals.

Figures 4b and 4c compare the recorded $S_{1750}P$ signal (see Figure 3c) to synthetic waveforms for different block thicknesses h and shear-velocity anomalies δV_S. The block thickness h controls the travel times of the entry and exit conversions and therefore the pulse width of $S_{1750}P$. The synthetics for $h = 2$ km and $h = 20$ km clearly underestimate and overestimate the recorded pulse width, respectively (Figure 4b). We find the best match for $h = 10$ km and use this value in our modeling. The shear-velocity anomaly δV_S of the block determines the polarity of δV_S. A negative value for δV_S is required to reproduce the down-and-up swing of $S_{1750}P$ (Figure 4c).

Figure 5 compares the recorded peak-to-peak amplitude of 4.4 ± 3.4% to predicted amplitudes when varying δV_S (in Figure 5a) and block angle α (in Figure 5b). The amplitude of $S_{1750}P$ depends linearly on δV_S. A value of $\delta V_S = -7\%$ produces a match between the computed and recorded mean peak-to-peak amplitude of $S_{1750}P$ but values of δV_S between -1.6% and -12.4% match the amplitude within its uncertainty range. The amplitude of $S_{1750}P$ depends on α in a non-linear manner. The predicted $S_{1750}P$ amplitude is highest when $\alpha \approx 10°$. Changing α by 20° decreases the $S_{1750}P$ amplitude by as much as 30%.

4 Discussion and Conclusions

If small-scale heterogeneities that produce high-amplitude S*x*P signals are indeed fragments of mid-ocean ridge basalt (MORB) subducted into the lower mantle, the analysis of S*x*P waveforms can place important constraints on the elastic properties and composition of MORB at lower-mantle conditions.

There is consensus that the density of MORB is 0.5% to 2% higher than the ambient mantle over the entire lower mantle range [*Irifune & Ringwood*, 1987, 1993; *Hirose et al.*, 1999; *Litasov et al.*, 2004; *Ricolleau et al.*, 2010; *Irifune & Tsuchiya*, 2015, e.g.,]. However, high-pressure experiments on the elastic properties of MORB are challenging and available estimates are based on ab-initio modeling [e.g., *Xu et al.*, 2008; *Tsuchiya*, 2011; *Kawai & Tsuchiya*, 2012; *Kudo*, 2012].

SiO_2 is an important component in MORB and undergoes a phase transition from stishovite to an orthorhombic $CaCl_2$ structure at mid-mantle conditions. *Karki et al.* [1997] first calculated from first principles the elastic parameters of stishovite and $CaCl_2$ and found a decrease in shear velocity. *Tsuchiya et al.* [2004] predicted that silica would exist in the $CaCl_2$ structure at 75 GPa along the geotherm of a subducting slab. If present in subducting slabs, silica will undergo this phase transition and produce seismic heterogeneities commonly observed near subduction zones.

Tsuchiya [2011] estimated that V_S is between 0 and 2% lower than the shear velocity of a pyrolitic mantle at a depth of 1750 km due to a post-stishovite transition. He found V_P does not change appreciably. In constrast, *Xu et al.* [2008] did not include the effect of post-stishovite and reported that V_S in a pyrolitic mantle increases with increasing basalt fraction. The presence of aluminum in silica further softens both stishovite and $CaCl_2$ [e.g., *Bolfan-Casanova et al.*, 2009; *Lakshtanov et al.*, 2007]. Our observation occurs at 75 GPa at a temperature range of 1200–2000 K, well within the P-T conditions of $CaCl_2$ estimated by *Ono et al.* [e.g., 2002]; *Nomura et al.* [e.g., 2010].

The negative polarity of $S_{1750}P$ is a robust observation and implies that the heterogeneity that produces this arrival has a lower shear velocity than the ambient mantle. The mean amplitude of $S_{1750}P$ indicates that δV_S is between -1.6% and -12.4%. This estimate is uncertain because the recorded $S_{1750}P$ amplitude is highly variable and the modeling is influenced by the geometry and orientation of the heterogeneity. However, the lowest value (i.e., -1.6%) for our estimate of δV_S is consistent with the shear-velocity reduction of MORB at deep mantle pressures, estimated by *Tsuchiya* [2011] as shown in Figure 4. We therefore interpret $S_{1750}P$ as a S-wave to P-wave conversion by a small-scale, MORB fragment in a subducted slab in the lower mantle beneath the Brazil earthquake. The relatively low shear-velocity of the MORB fragment is evidence for shear softening due to the post-sitshovite phase transition in MORB in the deep mantle.

Seismological modeling of $S_{1750}P$ can benefit from additional broadband recordings to constrain waveform polarity and amplitude variability. In addition, estimates of the seismic properties of subducted MORB in the lower mantle will improve if we can consider the effects of off-azimuth wave propagation and SH-to-P wave conversions contributing to $S_{1750}P$. This requires computational resources that are currently not available to us.

Acknowledgments

This research was funded by the National Science Foundation under grant EAR–1644829. We acknowledge the University of Utah Center for High Performance Computing (CHPC) for computer resources and support. Michael S. Thorne was partially supported by NSF grant EAR–1401097. Seismic data have been provided by the Incorporated Research Institutions for Seismology (IRIS) and the Geological Survey of Canada. We thank Jennifer Jenkins and an anonymous reviewer for helpful comments. We thank Editor Noah Diffenbaugh for overseeing the editorial process.

References

Bolfan-Casanova, N., Andrault, D., Amiguet, E., & Guignot, N. (2009). Equation of state and post-stishovite transformation of Al-bearing silica up to 100GPa and 3000K. *Physics of the Earth and Planetary Interiors*, 174(1), 70–77. https://doi.org/10.1016/j.pepi.2008.06.024

Castle, J. C., & van der Hilst, R. D. (2003). Searching for seismic scattering off mantle interfaces between 800 km and 2000 km depth, *Journal of Geophysical Research*, 108, 2095. https://doi.org/10.1029/2001JB000286

Fukao, Y., S. Widiyantoro, & Obayashi, M. (2001). Stagnant slabs in the upper and lower mantle transition region, *Reviews of Geophysics*, 39(3), 291–323. https://doi.org/doi:10.1029/1999RG000068

Grand, S. P., van der Hilst, R. D., & Widiyantoro, S. (1997). High resolution global tomography: a snapshot of convection in the Earth. *Geological Society of America Today*, 7(4).

Hirose, K., Fei, Y., Ma, Y., & Mao, H. K. (1999). The fate of subducted basaltic crust in the Earth's lower mantle. *Nature*, 397(6714), 53–56. https://doi.org/10.1038/16225

Irifune, T., & Tsuchiya, T. (2007). Mineralogy of the Earth–Phase Transitions and Mineralogy of the Lower Mantle, *Treatise on Geophysics, 2* 33–62. https://doi.org/10.1029/2012JB009696

Irifune, T., & Ringwood, A. E. (1987). Phase transformations in a harzburgite composition to 26 GPa: implications for dynamical behaviour of the subducting slab. *Earth and Planetary Science Letters*, 86(2-4), 365–376. https://doi.org/10.1016/0012-821X(87)90233-0

Irifune, T., & Ringwood, A. E. (1993), Phase transformations in subducted oceanic crust and buoyancy relationships at depths of 600–800 km in the mantle. *Earth and Planetary Science Letters*, 117(1–2), 101–110. https://doi.org/10.1016/0012-821X(93)90120-X

Jahnke, G., Thorne, M. S., Cochard, A., & Igel, H. (2008). Global SH-wave propagation using a parallel axisymmetric spherical finite-difference scheme: application to whole mantle scattering. *Geophysical Journal International*, 173(3), 815–826. https://doi.org/10.1111/j.1365-246X.2008.03744.x

Kudo, Y., Hirose, K., Murakami, M., Asahara, Y., Ozawa, H., Ohishi, Y., & Hirao, N. (2012). Sound velocity measurements of $CaSiO_3$ perovskite to 133GPa and implications for lowermost mantle seismic anomalies. *Earth and Planetary Science Letters*, 349, 1–7. https://doi.org/10.1016/j.epsl.2012.06.040

Kaneshima, S. (2013). Lower mantle seismic scatterers below the subducting Tonga slab: Evidence for slab entrainment of transition zone materials. *Physics of the Earth and Planetary Interiors*, 222, 35–46. https://doi.org/10.1016/j.pepi.2013.07.001

Kaneshima, S. (2016). Seismic scatterers in the mid-lower mantle. *Physics of the Earth and Planetary Interiors*, 257, 105–114. https://doi.org/10.1016/j.pepi.2016.05.004

Kaneshima, S., & Helffrich, G. (1998). Detection of lower mantle scatterers northeast of the Marianna subduction zone using short-âĂŘperiod array data. *Journal of Geophysical Research: Solid Earth*, 103(B3), 4825–4838. https://doi.org/10.1029/97JB02565

Kaneshima, S., & Helffrich, G. (1999). Dipping low-velocity layer in the mid-lower mantle: evidence for geochemical heterogeneity. *Science*, 283(5409), 1888–1892. https://doi.org/10.1126/science.283.5409.1888

Kaneshima, S., & Helffrich, G. (2003). Subparallel dipping heterogeneities in the midâĂŘlower mantle. *Journal of Geophysical Research: Solid Earth*, 108(B5). https://doi.org/10.1029/2001JB001596

Kaneshima, S., & Helffrich, G. (2010). Small scale heterogeneity in the mid-lower mantle beneath the circum-Pacific area. *Physics of the Earth and Planetary Interiors*, 183(1), 91–103. https://doi.org/10.1016/j.pepi.2010.03.011

Karki, B. B., Stixrude, L., & Crain, J. (1997). Ab initio elasticity of three highâĂŘ-pressure polymorphs of silica. *Geophysical Research Letters*, 24(24), 3269-3272. https://doi.org/10.1029/97GL53196

Kawai, K., & Tsuchiya, T. (2012). First principles investigations on the elasticity and phase stability of grossular garnet. *Journal of Geophysical Research: Solid Earth*, 117(B2). https://doi.org/10.1029/2011JB008529

Kawakatsu, H., & Niu, F. (1994). Seismic evidence for a 920-km discontinuity in the mantle. Nature, 371(6495), 301–305. https://doi.org/10.1038/371301a0

Lakshtanov, D. L., Sinogeikin, S. V., Litasov, K. D., Prakapenka, V. B., Hellwig, H., Wang, J., ... Li, J. (2007). The post-stishovite phase transition in hydrous alumina-bearing SiO2 in the lower mantle of the Earth. *Proceedings of the National Academy of Sciences*, 104(34), 13588–13590. https://doi.org/10.1073/pnas.0706113104

Li, J., & Yuen, D. A. (2014). Mid-mantle heterogeneities associated with Izanagi plate: Implications for regional mantle viscosity. *Earth and Planetary Science Letters*, 385, 137–144. https://doi.org/10.1016/j.epsl.2013.10.042

Litasov, K., Ohtani, E., Suzuki, A., Kawazoe, T., & Funakoshi, K. (2004). Absence of density crossover between basalt and peridotite in the cold slabs passing through 660 km discontinuity. *Geophysical Research Letters*, 31(24). https://doi.org/10.1029/2004GL021306

Niu, F. (2014). Distinct compositional thin layers at mid-mantle depths beneath northeast China revealed by the USArray. *Earth and Planetary Science Letters*, 402, 305–312. https://doi.org/10.1016/j.epsl.2013.02.015

Niu, F., & Kawakatsu, H. (1997). Depth variation of the midâĂŘmantle seismic discontinuity. *Geophysical Research Letters*, 24(4), 429–432. https://doi.org/10.1029/97GL00216

Nomura, R., Hirose, K., Sata, N., & Ohishi, Y. (2010). Precise determination of post-stishovite phase transition boundary and implications for seismic heterogeneities in the mid-lower mantle. *Physics of the Earth and Planetary Interiors*, 183(1), 104–109. https://doi.org/10.1016/j.pepi.2010.08.004

Ono, S., Hirose, K., Murakami, M., & Isshiki, M. (2002). Post-stishovite phase boundary in SiO2 determined by in situ X-ray observations. *Earth and Planetary Science Letters*, 197(3), 187–192. https://doi.org/10.1016/S0012-821X(02)00479-X

Ricolleau, A., Perrillat, J. P., Fiquet, G., Daniel, I., Matas, J., Addad, A., ... Guignot, N. (2010), Phase relations and equation of state of a natural MORB: Implications for the density profile of subducted oceanic crust in the Earth's lower mantle. *Journal of Geophysical Research: Solid Earth*, 115(B8). https://doi.org/10.1029/2009JB006709

Ritsema, J., Deuss, A. A., Van Heijst, H. J., & Woodhouse, J. H. (2011). S40RTS: a degree-40 shear-velocity model for the mantle from new Rayleigh wave dispersion, teleseismic traveltime and normal-mode splitting function measurements. *Geophysical Journal International*, 184(3), 1223–1236. https://doi.org/10.1111/j.1365-246X.2010.04884.x

Shearer, P. M. (2007). Deep Earth Structure–Seismic Scattering in the Deep Earth. *Treatise on Geophysics*, 1.20.

Thorne, M. S., Zhang, Y., & Ritsema, J. (2013). Evaluation of 1âĂŘD and 3âĂŘD seismic models of the Pacific lower mantle with S, SKS, and SKKS traveltimes and amplitudes. *Journal of Geophysical Research: Solid Earth*, 118(3), 985–995. https://doi.org/10.1002/jgrb.50054

Tsuchiya, T. (2011). Elasticity of subducted basaltic crust at the lower mantle pressures: Insights on the nature of deep mantle heterogeneity. *Physics of the Earth and Planetary Interiors*, 188(3), 142–149. https://doi.org/10.1016/j.pepi.2011.06.018

Tsuchiya, T., Caracas, R., & Tsuchiya, J. (2004). First principles determination of the phase boundaries of highâĂŘpressure polymorphs of silica. *Geophysical Research Letters*, 31(11). http://doi.org/10.1029/2004GL019649

Vanacore, E., Niu, F., & Kawakatsu, H. (2006). Observations of the midâĂŘmantle discontinuity beneath Indonesia from S to P converted waveforms. *Geophysical Research Letters*, 33(4). https://doi.org/10.1029/2005GL025106

Vinnik, L., Niu, F., & Kawakatsu, H. (1998). Broadband converted phases from midmantle discontinuities. *Earth, Planets and Space*, 50(11–12), 987–997. http://doi.org/10.1186/BF03352193

Xu, W., Lithgow-Bertelloni, C., Stixrude, L., & Ritsema, J. (2008). The effect of bulk composition and temperature on mantle seismic structure. *Earth and Planetary Science Letters*, 275(1), 70–79. https://doi.org/10.1016/j.epsl.2008.08.012

Yang, Z., & He, X. (2015). Oceanic crust in the mid-mantle beneath west-central Pacific subduction zones: evidence from S to P converted waveforms. Geophysical Journal International, 203(1), 541–547. https://doi.org/10.1093/gji/ggv314

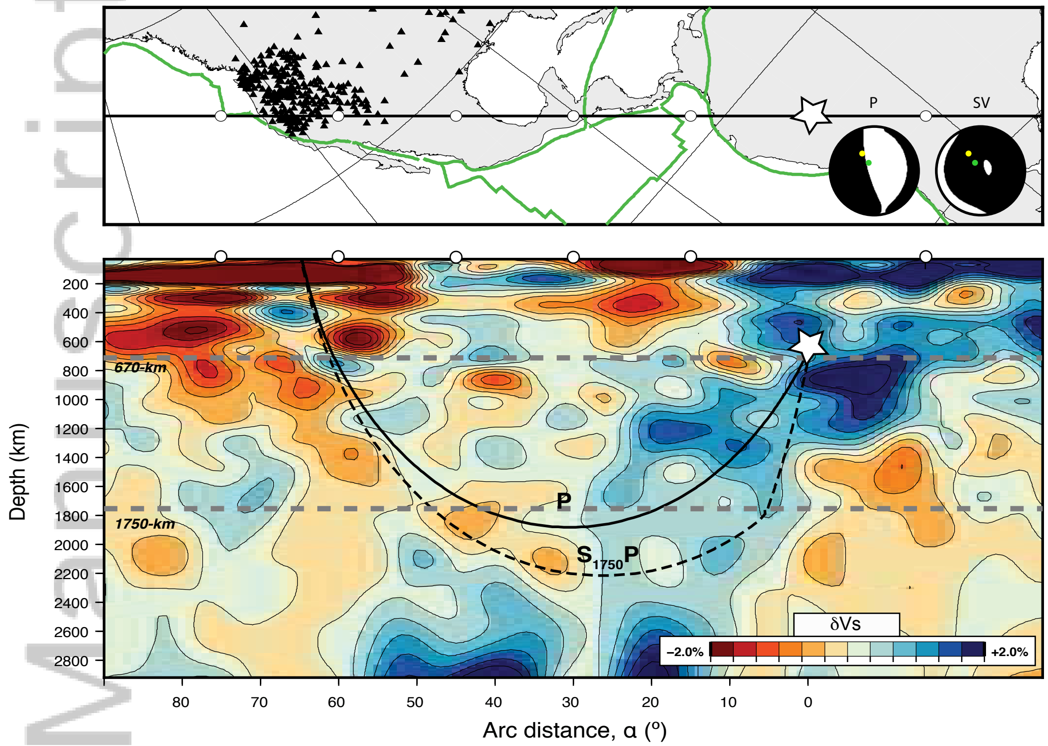

Figure 1. (top) Source-receiver geometry of the July 10, 2007 western Brazil earthquake. The star indicates the epicenter. The triangles indicate the locations of stations from the Transportable Array (TA) and the Canadian National Seismic Network (CNSN) used in the analysis. The black line is great-circle arc through the Brazil event and the western US. The white circles on top are drawn every 15°. P-wave and SV-wave radiation patterns are shown on the lower right. Green circles on the radiation pattern indicate the $S_{1750}P$ take-off direction. Yellow circles on P and SV radiation patterns indicate P and S wave take-off directions, respectively. (bottom) Geometric ray paths of P (solid line) and $S_{1750}P$ (dashed line) for an epicentral distance of 65°. The ray paths are superposed on a NW–SE oriented cross-section of the S40RTS model [*Ritsema et al.*, 2011] through the Brazil event and the TA and CNSN stations. Note that $S_{1750}P$ is formed within a high-velocity anomaly in the lower mantle beneath South America.

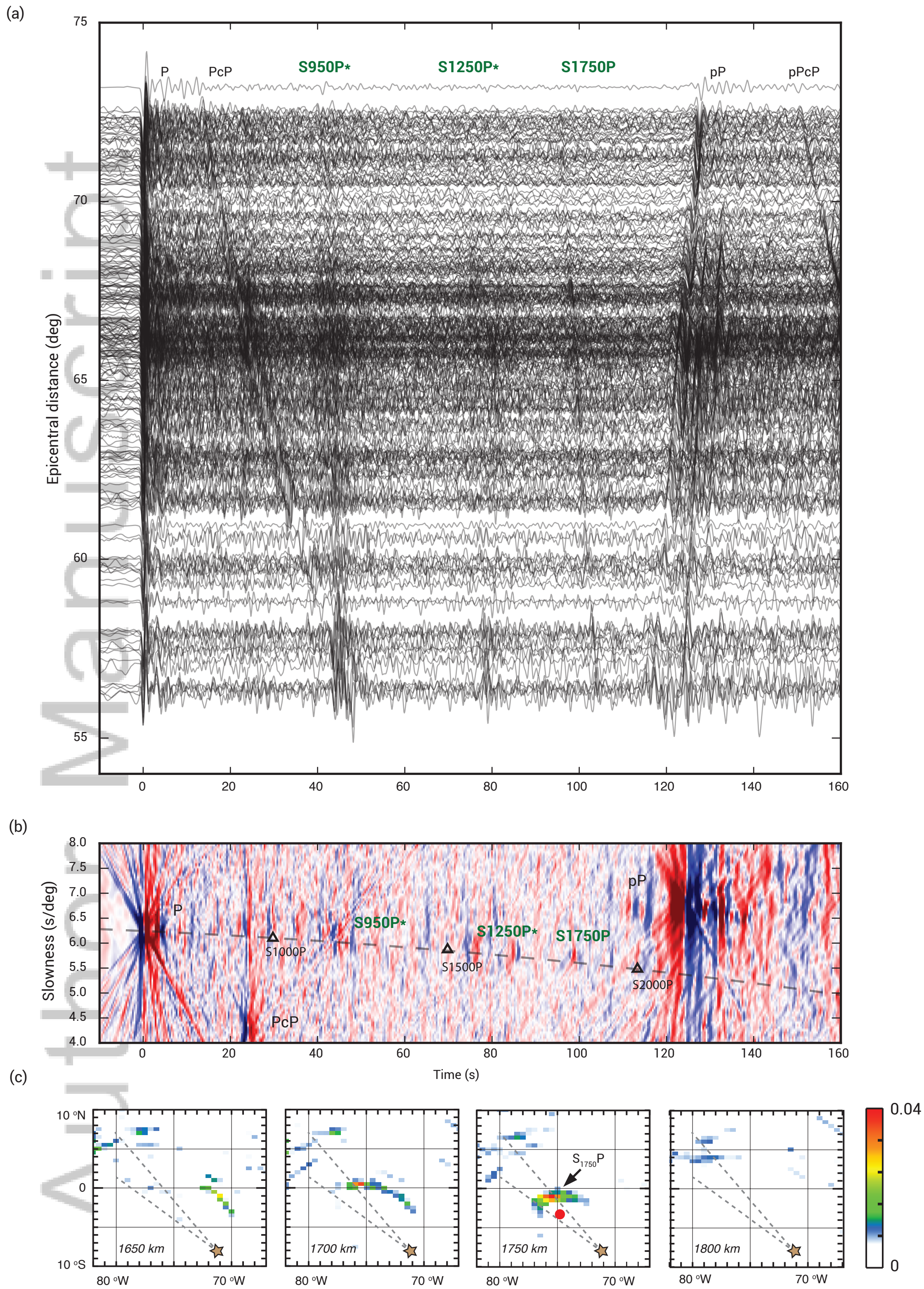

Figure 2. (a) Record section of velocity waveforms of the Brazil event aligned on the P-wave arrival (at time 0). Labeled on top are the arrival times of the major phases P, PcP, pP, pPcP, and S-P conversions at 950 km, 1250 km and 1750 km depth. The conversion depths of $S_{950}P$ and $S_{1250}P$ are shallower depth than expected for 1-D models for their traveltimes because these phases propagate off-azimuth for the Brazil earth-

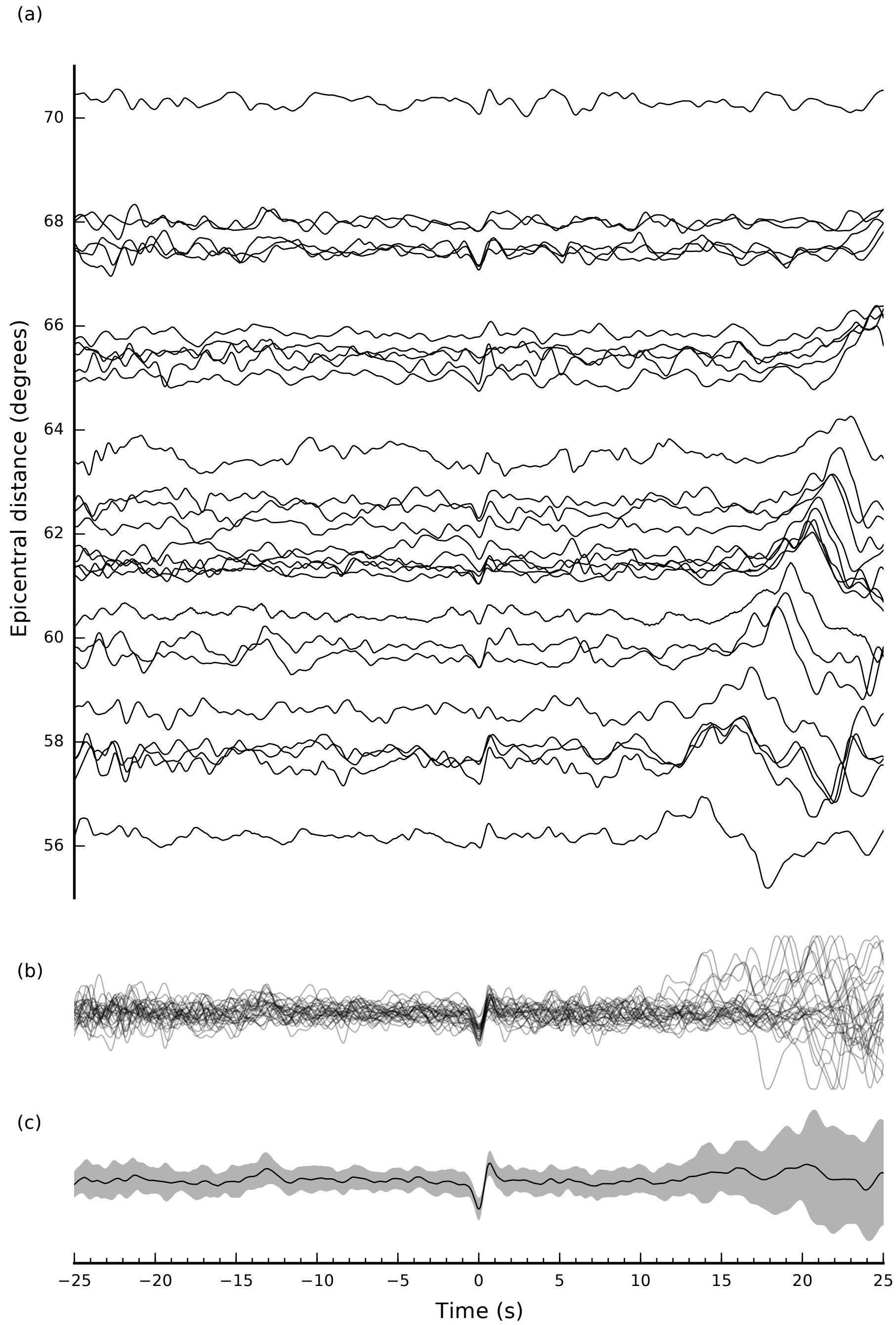

Figure 3. (a) Record section and (b) stacked displacement waveforms centered on $S_{1750}P$ from 30 TA and CNSN stations. The large amplitude signal moving out with increasing distance is pP. (c) Sum of the displacement waveforms. The grey envelope is two standard deviations wide and indicates amplitude variability present in the data.

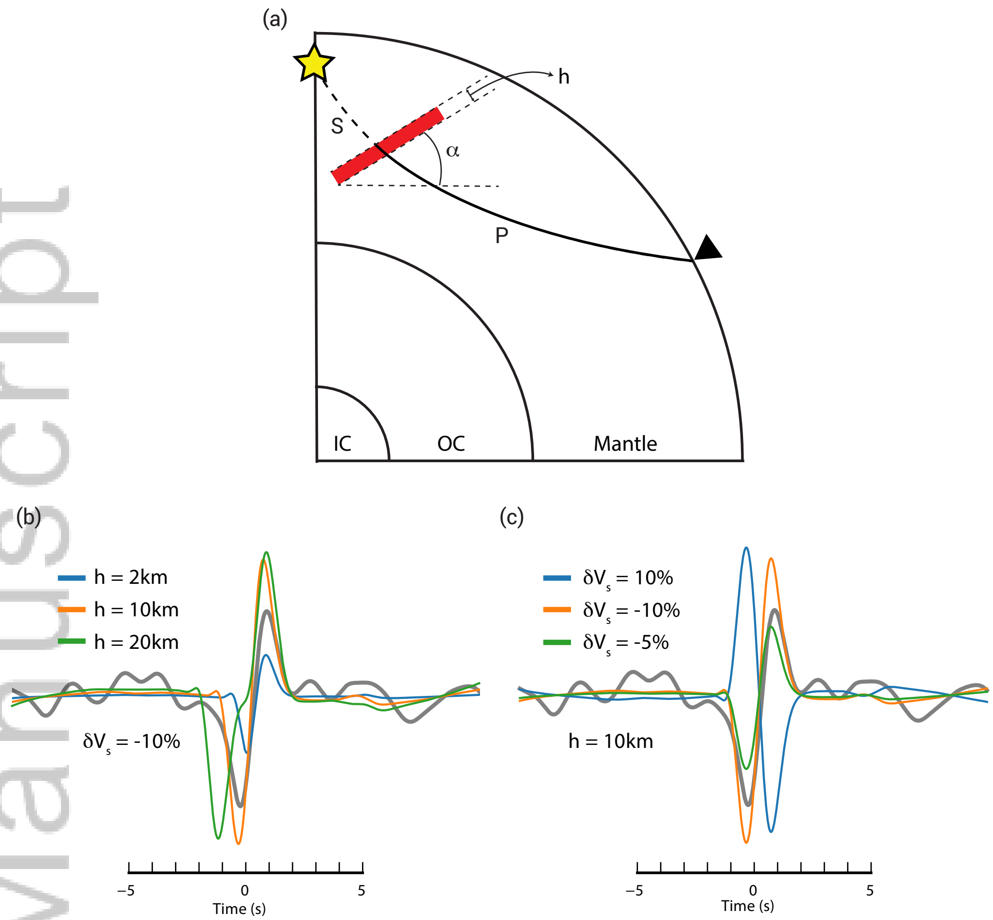

Figure 4. (a) Illustration of the model. The heterogeneity responsible for forming $S_{1750}P$ is modeled as a block at 1750 km depth with a thickness h that makes an angle α with the equatorial plane. It has a velocity contrast δV_S with respect to the ambient mantle. (b) Synthetic waveforms for $h = 2$ km, $h = 10$ km, and $h = 20$ km. δV_S = -10% in these simulations. (c) Synthetic waveforms for $\delta V_S = 10\%$, $\delta V_S = -10\%$, and $\delta V_S = -5\%$. $h = 10$ km in these simulations. For all simulations in (b) and (c) $\alpha = 0°$, the epicentral distance is 65°, and the grey waveform is the stack of the recorded $S_{1750}P$ waveforms.

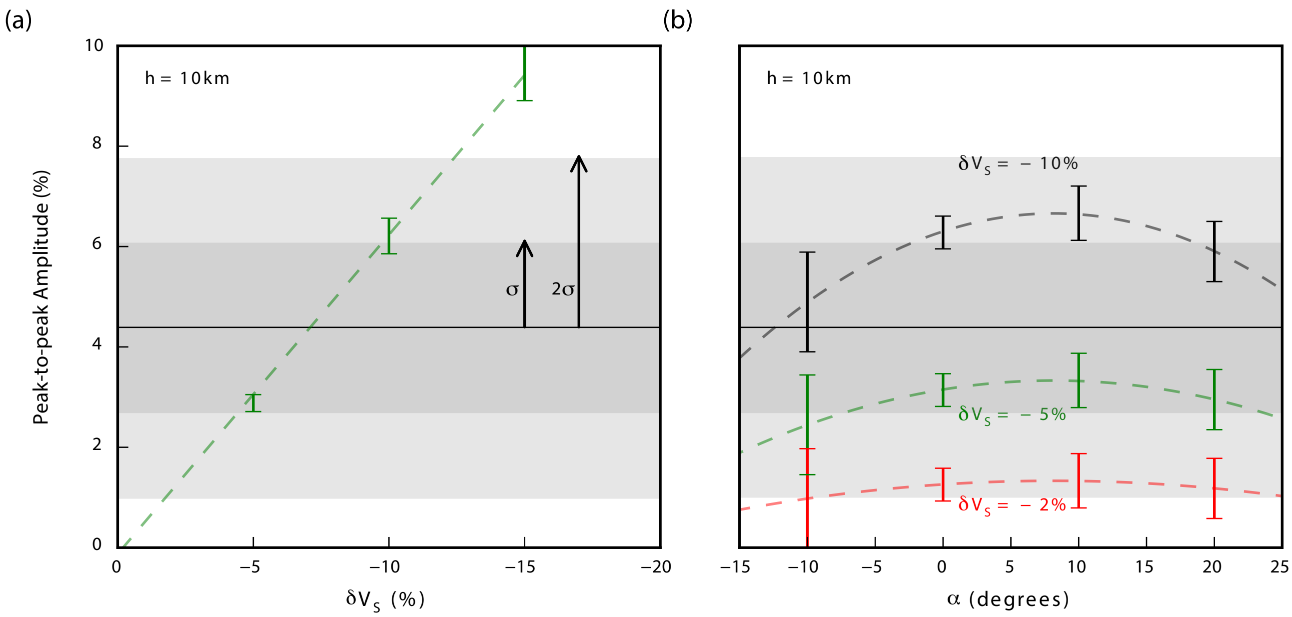

Figure 5. Peak-to-peak $S_{1750}P$ amplitude normalized to the radial SV component as a function of (a) δV_S and (b) block angle α. The horizontal black line indicates the mean value of the amplitude. Its two grey envelopes are one- and two-standard deviations wide. Vertical black bars are predicted amplitudes with error bars estimated from the minimum and maximum values for a range of epicentral distances.

Figure 1.

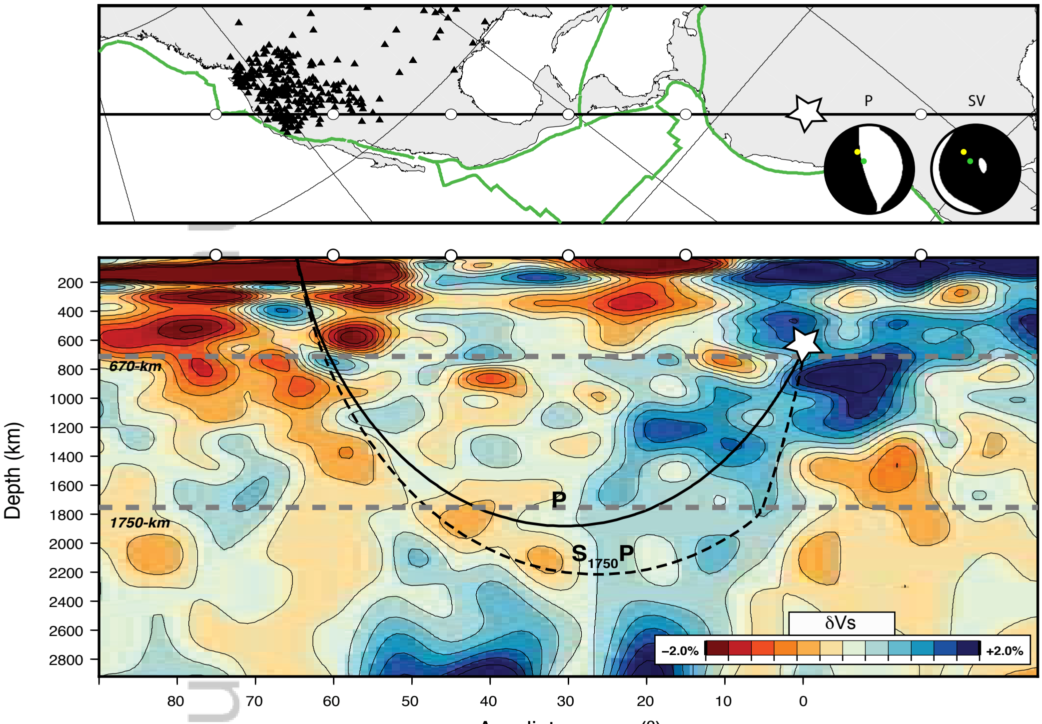
P
SV
200
400
600
800
1000
1200
1400
1600
1800
2000
2200
2400
2600
2800
Depth (km)
670-km
1750-km
P
$S_{1750}P$
δVs
−2.0%
+2.0%
80
70
60
50
40
30
20
10
0
Arc distance, α (°)

Figure 2.

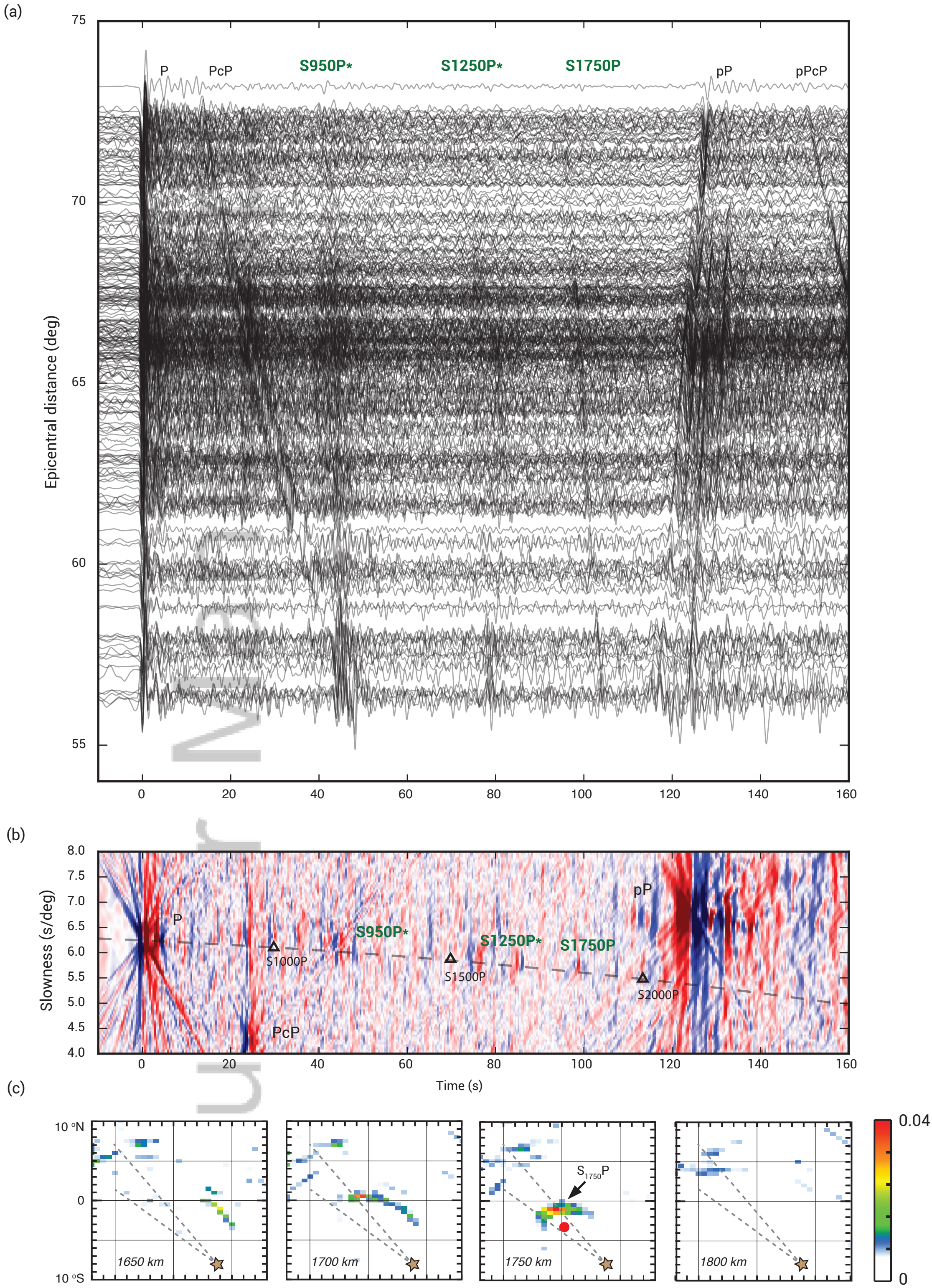
(a)
P
PcP
S950P*
S1250P*
S1750P
pP
pPcP
Epicentral distance (deg)
(b)
Slowness (s/deg)
S1000P
S1500P
S2000P
Time (s)
(c)
1650 km
1700 km
1750 km
1800 km
S1750P
10 °N
0
10 °S
80 °W
70 °W
0.04
0

Figure 3.

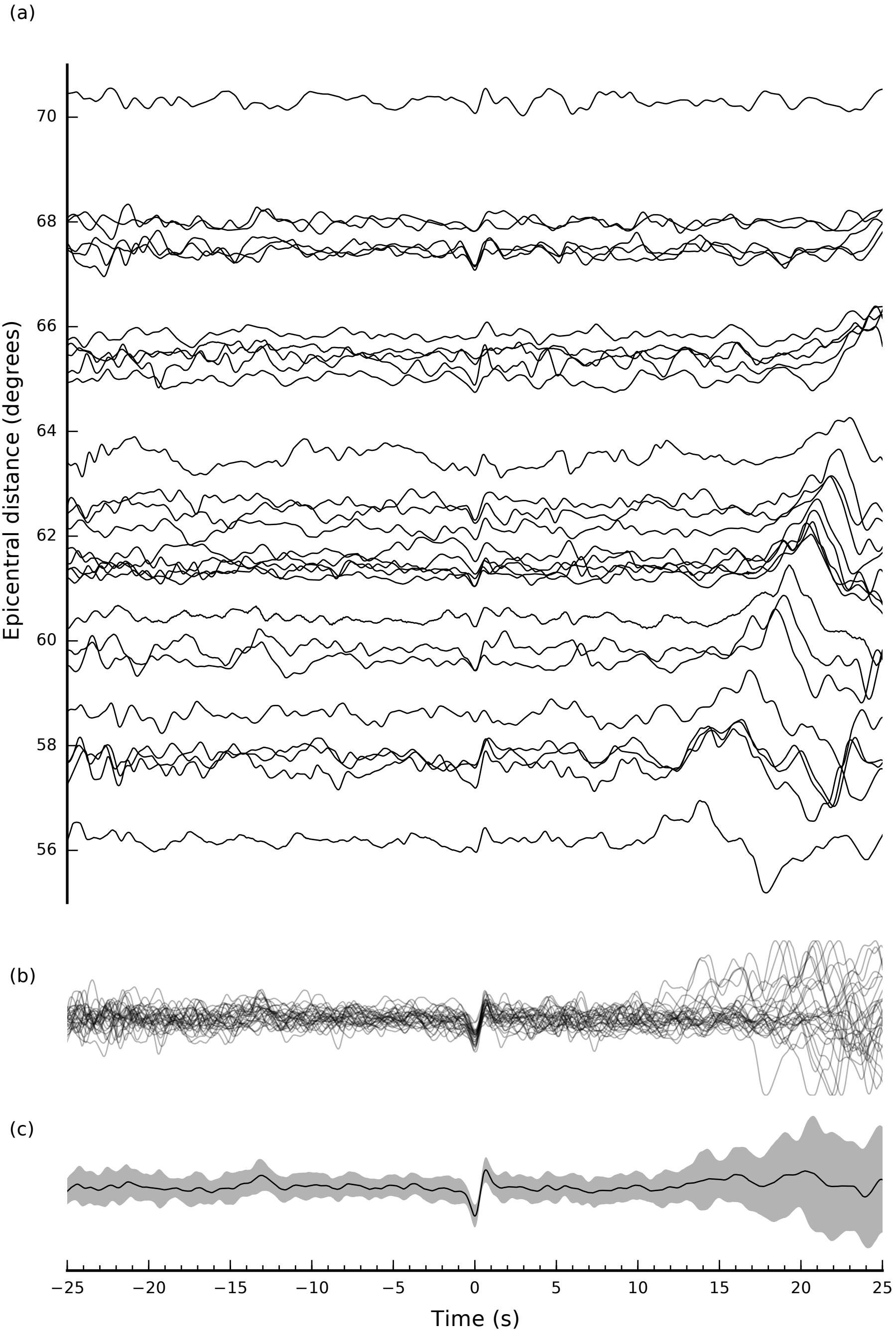
(a)
70
68
66
64
62
60
58
56
Epicentral distance (degrees)
(b)
(c)
−25
−20
−15
−10
−5
0
5
10
15
20
25
Time (s)

Figure 4.

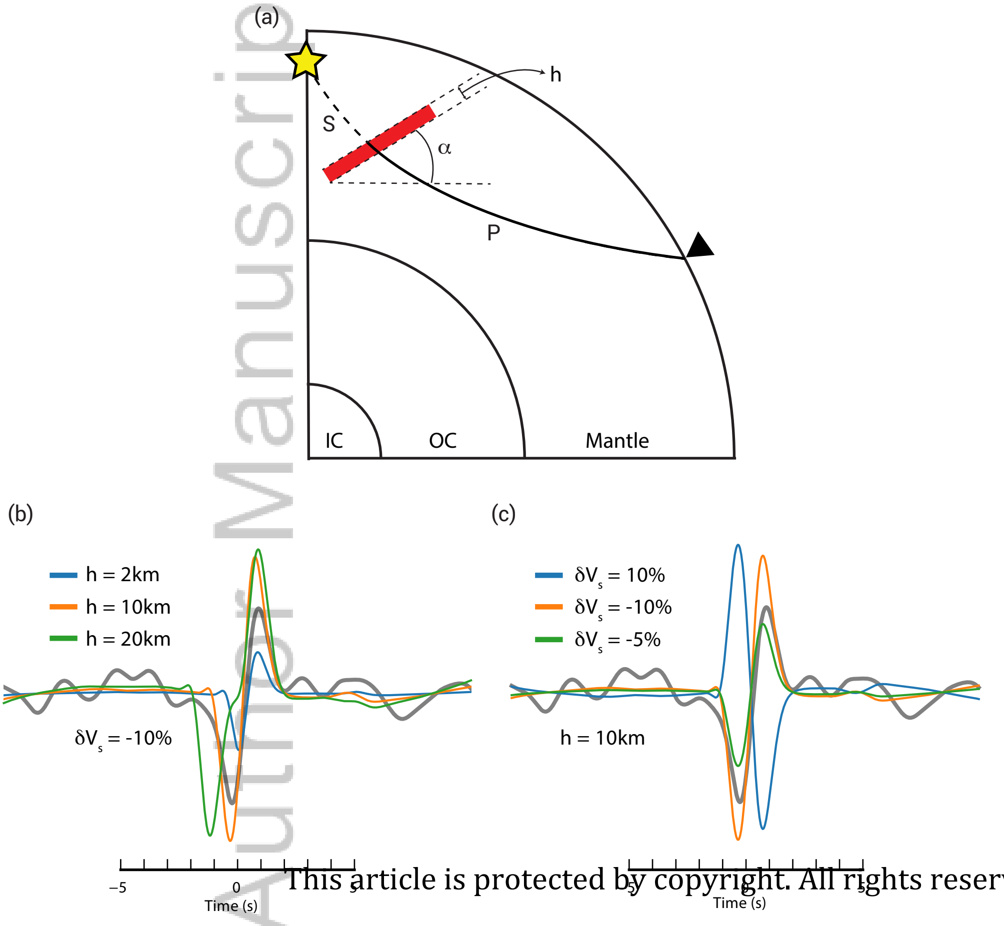
(a)
h
S
α
P
IC
OC
Mantle
(b)
h = 2km
h = 10km
h = 20km
δV_s = -10%
−5
0
5
Time (s)
(c)
δV_s = 10%
δV_s = -10%
δV_s = -5%
h = 10km
−5
0
5
Time (s)

Figure 5.

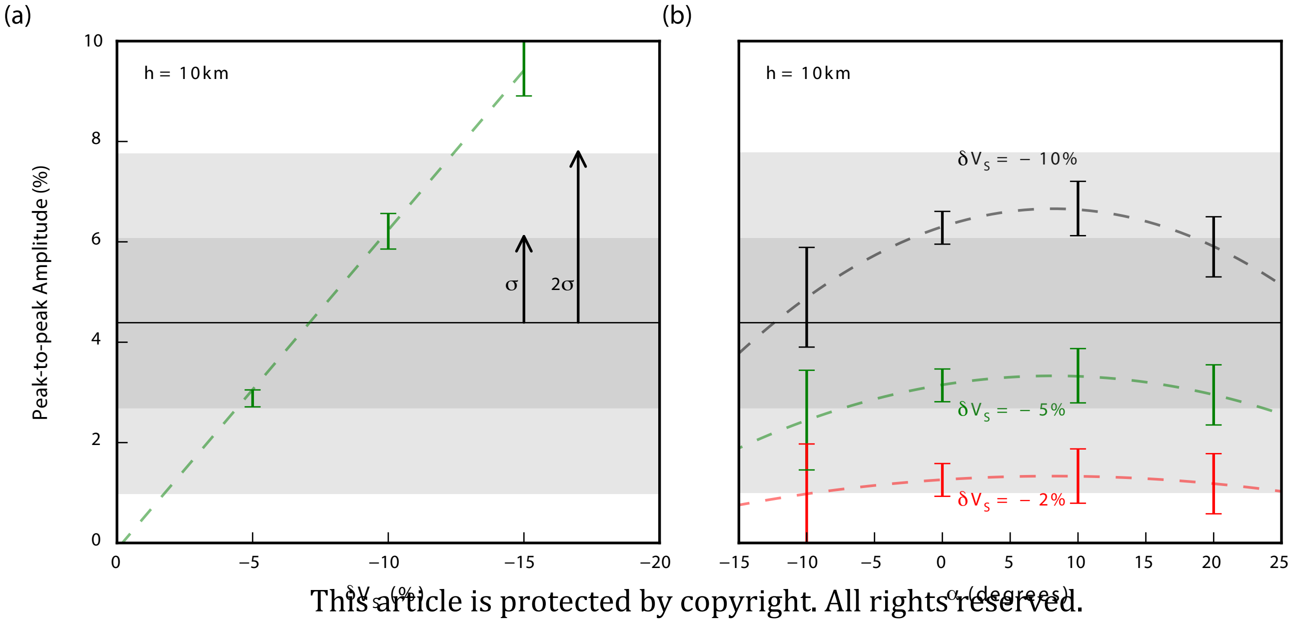

(a)
(b)
h = 10km
h = 10km
σ
2σ
δV_S = − 10%
δV_S = − 5%
δV_S = − 2%
Peak-to-peak Amplitude (%)
δV_S (%)
α (degrees)